J. Min. Metall. Sect. B-Metall. 53 (1) B (2017) 19 - 29

Journal of Mining and Metallurgy, Section B: Metallurgy

COMPARISON OF THE MINERALOGY AND MICROSTRUCTURE OF EAF STAINLESS STEEL SLAGS WITH REFERENCE TO THE COOLING TREATMENT

M. Loncnar[a,*], A. Mladenovič[b], M. Zupančič[c], P. Bukovec[c]

[a] Acroni, d. o. o., Jesenice, Slovenia
[b] Slovenian National Building and Civil Engineering Institute, Ljubljana, Slovenia
[c] Faculty of Chemistry and Chemical Technology, University of Ljubljana, Ljubljana, Slovenia

(Received 10 September 2015; accepted 23 June 2016)

Abstract

TIn the present study the differences in the mineralogical composition and microstructure of various types of EAF stainless steel (EAF S) slag with regard to the cooling treatment, the operation practice in an EAF (electric arc furnace) and environmental ageing reactions were evaluated. It was shown that the mineralogy of the investigated EAF S slags varied from one slag to another, depending on the quality of the produced stainless steel. The production process of the treated steel also has a strong influence on the mineralogy of the slags. The conditions during water cooling treatment were not sufficient to prevent the crystallization of primary mineral phases, which occurs predominantly in air-cooled EAF S slags, probably due to the high basicity of the investigated slags. However, the water cooling treatment of hot slag leads to the absence of γ-$CaSiO_4$ and the formation of secondary mineral phases predominantly calcite, portlandite, ettringite, calcium aluminate hydrate and calcium silicate hydrate. It has been shown that during the environmental ageing test (down-flow column test) secondary mineral phases were formed, which were the same as those formed during the water cooling treatment.

***Keywords**: Electric arc furnace stainless steel slag; Cooling path; Microstructure; Mineralogy*

1. Introduction

EAF stainless steel (EAF S) slags are a by-product of the primary steel-making process in an electric arc furnace (EAF). The annual amount of produced EAF S slags in the Europe in year 2010 was 1.74 million tonnes [1], which present enormity annual quantities for dumping. In spirit of zero-waste assessment the use of EAF S slags has priority before dumping.

In recent years methods of slag treatment have been increasingly studied. The main aim has been to obtain a valuable product from the slag. Slag treatments focus on the hot stage processing of slags, i.e. from the moment of slag/metal separation to complete cooling at the slag yard. Studies have focused on additions during the molten state, on variations of the cooling path, and on their influence on the microstructure and properties of solidified slags [2]. The amount of slag which can be used is, in the case of slow air cooling treatment, much less than the amount of slag which is stabilized by water cooling treatment. This is mostly due to the partially disintegration of slag upon air-cooling treatment [2], and/or volume instability due to the hydration of free CaO and MgO to $Ca(OH)_2$ and $Mg(OH)_2$ [3]. In the field, the stabilization of steel slag can (with the aim of achieving better technical properties) take from a couple of days (if accelerated ageing by means of steam injection is used) up to several months.

In this research, detailed mineralogical characterization of EAF S slags exposed to different cooling treatment (slow air cooling treatment or fast water cooling treatment) was performed. The water cooling treatment of hot slags is, from the technical point of view, an easily feasible way to enhance the stabilization of EAF S slag. The purpose of the study was to investigate the mineralogy of coarse EAF S slag samples, since this gradation of EAF S slag has the potential to be used as an artificial aggregate for civil engineering purposes. The mineralogy of EAF S slags is one of the key factors in the study of this potential since unstable mineral phases, which may be present in the slag, are identified. Since EAF S slags contain higher amount of chromium oxide, special attention needs to be paid to the identification and recognition of the mineral phases with chromium.

* *Corresponding author: mojca.loncnar@acroni.si*

DOI:10.2298/JMMB150910018L

Considering that the formation of secondary mineral phases has an effect on the release of contaminants [4], attention was also paid in this study to the formation of secondary mineral phases. Detail mineralogy of the slags exposed to the down-flow column test were performed in order to get a better insight into the ageing process of EAF S slag. Since technical process of steel production may effect slag mineralogy, the slag sampling was done at two different operation practice in an EAF.

2. Materials and methods

2.1 Materials

The EAF S steel slags were obtained from a Slovenian steel plant ACRONI d.o.o., which was designed to produce stainless steel from scrap steel. All the samples originated from stainless steel production. In the first part of the study three austenitic steel slags (steel grades: X2 CrNi 18-9 (samples E_A1Ac and E_A1Wq), AlSi 304 (samples E_A2Ac and E_A2Wi) and AlSi 316 L (samples E_A3Ac and E_A3Wq)) and one ferritic steel slag (steel grade MKM CrAl 4 (samples E_FAc and E_FWq)) were sampled. In the second part three additional slags originating from steel grade X2 CrNi 18-9 were investigated, two of them obtained from normal operation practice in an EAF (samples E_1A1Ac, E_1A1Wi, E_1A1Wq and E_2A1Ac, E_2A1Wi1, E_2A1Wi2, E_2A1Wq1, E_2A1Wq2), and one from a CaC_2 injection operation (samples E_A1CaC2Ac, E_A1CaC2Wi and E_A1CaC2Wq) in order to study the variation in slag composition within the same steel grade. The trials performed with the CaC_2-mix injection were performed within the scope of the EU project: "EPOSS" [5]. In the EPOSS project the slag conditioning technique in an EAF by the addition/injection of CaC_2 as the main reducer was evaluated, whereas slag mineralogy was evaluated in this study. Slag sampling was performed at the end of the metallurgical process in an EAF, immediately after the liquid slag had been poured from the ladle into the pit beneath the furnace. One part of the fresh (hot) slag was left to cool at ambient temperature for 24 hours, whereas another part was rapidly water cooled. In the first part of the study slags were water quenched (Wq), with the exception of slag the originating from steel grade AlSi 304, which was cooled by immersion into a bucket of water (Wi), whereas in the second part of the study all the slags were cooled by means of both water cooling treatment either by water quenching or by immersion. The samples (each with a weight of approximately 10 kg) were crushed to a size of less than 10 mm, in accordance with the provisions of SIST EN 12457-4:2004 [6]. The chemical composition and leaching properties of the EAF S slags sampled in the first part of the study were studied by means of the standardized one-stage batch test according to SIST EN 12457-4:2004 [6] (24 h water extraction of the slag samples at an L/S ratio of 10), by Loncnar et al. [7]. The additional samples E_A1Ac and E_A1Wq were subject to down-flow column tests using a synthetic leaching solution (USEPA (2008) Method 1312) [8]. The slags recovered from the down-flow column tests were designated E_A1Ac* and E_A1Wq*, respectively. The down-flow column test was performed in order to get a better insight into the ageing process of EAF S slag, taking into account the fact that unsaturated intermittent flow can produce conditions (e.g. carbonation, oxidation) which are more comparable to those occurring in the field.

2.2 Mineralogical and microstructure characterization

X-ray diffraction (XRD) was used to identify the main mineral phases in the slag. A PANalytical X'Pert PRO diffractometer was used, operating at 45 kV and 40 mA, using Cu Kα1 (1.5406 Å) radiation, with an acquisition interval of 5–80° (2θ) and a step size of 0.02°.

The microstructure of the slag was analyzed, on polished samples that were prepared from the selected gradation (1.0–4.0) mm, in a JEOL 5500 LV scanning electron microscope (SEM) coupled to an Oxford energy dispersive spectrometer (EDS), using backscattered electrons (BSE) and the low vacuum mode. The equipment conditions were as follows: an acceleration voltage of 20 kV, a working distance of 20 mm, and a working pressure of 10–20 Pa. Additional analysis of slag surface were perform on slag grains (1–10 mm) before and after exposure to the down-flow column test (samples E_A1Ac, E_A1Wq, E_A1Ac* and E_A1Wq*).

2.3 Mechanical and physical properties

The analysis of particle density, specific surface area and mesopores were done just on samples E_1A1Ac, E_1A1Wi, E_1A1Wq (steel grade: X2 CrNi 18-8; from normal operation practice in an EAF) and samples E_A1CaC2Ac, E_A1CaC2Wi, E_A1CaC2Wq (steel grade: X2 CrNi 18-8; a CaC_2 injection operation), whereas the particle size distribution was done on all samples on particle size 0 –10 mm according to the SIST EN 933-1:1999/A1:2005 [9]. Determination of particle density was done on fraction 0/4 mm and 4/10 in petroleum according to the SIST EN 1097-7:2008 [10]. Specific surface area and analysis of mesopores by gas adsorption was done according to the ISO 15901-2:2006 [11].

3. Results and discussion

3.1 Slag composition

It was observed certain variation within chemical composition of investigated EAF S slags (Table 1). Just a small variation (less than 10 %) of the major components in the water-cooled slag samples was observed, leading to the conclusion that only a slight dissolution of the major elements occurred during the water cooling treatment. Exceptionally, in the case of iron and nickel, a more noticeable variation between the air- and water-cooled slag was observed due to the different content of metallic droplets, which, as will be shown later, were unevenly distributed in the slag samples. Similar just a small variation (within 10 %) of the major components in the slag before and after the down-flow column test was observed, leading to the conclusion that only a slight dissolution of the major elements had occurred during the down-flow column test. A more noticeable variation between the air- and water-cooled slag before and after the down-flow column test was observed in the case of carbon due to the carbonation of the samples (0.16 wt.% C in sample E_A1Ac, 0.23 wt.% C in sample E_A1Wq, 0.22 wt.% in sample E_A1Ac* and 0.26 wt.% C in sample E_A1Wq*).

All the investigated EAF S slags were basic (Table 1). There are several ways of expressing slag basicity. The simplest way is to express it as a relationship between CaO (the weight percentage of CaO) and SiO_2 (the weight percentage of CaO) [12], although it is preferable to also take into account the MgO and Al_2O_3 content, as proposed by Tossavainen et al. [13]. The average basicity of the investigated slags, expressed as B, was 2. This value is a bit higher than that reported by Mostafaee et al. [12], who determined that the average basicity of EAF S slag (steel batch: AlSi 304 L) was 1.5, and Vidacak et al. [14], where the determined slag basicity was between 1.5 and 1.7. The basicity of sample EM1 (B = 4.0) was higher than the values obtained in the case of the rest of the slag samples, due to the lower SiO_2 content in this slag sample (Table 1). If the MgO and Al_2O_3 contents are also taken into account when expressing slag basicity as M_b, the variation in the basicity of samples EM1 and EM2 is smaller (Table 1). The M_b index indicates a slightly lower basicity (on average 1.8) in comparison to the index B. In a study performed by Tossavainen et al. [13] the basicity of high alloy steel slag was a bit lower (Mb = 1.4) than in our case.

3.2 The mineral phases in the air-cooled EAF S slags

The X-ray diffraction (XRD) pattern of the air-cooled slag samples was, in general, very complex, showing many mineral species. At the same time certain variations within the investigated EAF S slags were observed (Table 2). XRD analysis revealed that the sample E_A2Ac was very similar to the sample E_A1Ac, although the former did also contain mayenite ($Ca_{12}Al_{14}O_{33}$), which was not identified in sample E_A1Ac. A comparison between the samples E_A1Ac and E_A3Ac revealed that the sample E_A3Ac did not contain γ-Ca_2SiO_4, nor there was any observable quantity of magnesium chromite. This was probably due to the fact that the content of Cr_2O_3 in sample E_A3Ac (5.9 wt.%) was half less than that in sample E_A1Ac (12.0 wt.% Cr_2O_3). Also, Mostafaee et al. [12] have reported that the Cr_2O_3 content has a strong effect on the formation of magnesium chromite in the EAF slag. The Cr_2O_3 content in the sample E_FAc was even lower (1.5 wt.%), so that no noticeable content of magnesium chromite was observed in the case of this sample. On the other hand, the sample E_FAc was rich in mayenite, which was also identified in smaller quantities, compared to sample E_FAc, in sample E_A2Ac. Tossavainen et al. [13] also found γ-Ca_2SiO_4 in original and semi-rapid cooled EAF slags. Beside γ-Ca_2SiO_4 merwinite, a solid solution spinel phase $(Mg, Mn)(Cr, Al)_2O_4$ and gehlenite were identified as the main minerals in EAF high alloy steel slag, which is consistent with our data. Shen et al. [15] found that EAF S slags consisted mainly of bredigite, merwinite and some akermanite, and gehlenite.

Certain variation within mineralogy was observed for EAF S slag (stainless steel grade: X2 CrNi 18-9)

Table 1. *Chemical composition of investigated air-cooled EAF S slags. The given data are the averages of three measurements*

	CaO	SiO_2	Al_2O_3	MgO	Cr_2O_3	Fe	MnO	V_2O_5	Ba	Mo	basicity	
sample	c/wt.%								c/mg kg^{-1}		B	M_b
E_A1Ac	37.5	20.2	6.59	8.69	12	6.7	3.54	0.283	251	470	1.85	1.72
E_A2Ac	41.4	18.8	8.86	9.55	9.18	4.4	3.03	0.243	259	250	2.2	1.89
E_A3Ac	36.2	22.4	7.47	13.8	5.91	8	3.29	0.139	560	2100	1.62	1.68
E_FAc	43.6	10.8	15.6	10.7	1.54	10.6	1.45	0.042	309	158	4.04	2.06
E_A1CaC_2Ac	43.8	21.3	7.1	10.1	4.6	4.9	1.61	0.257	820	240	2.06	1.9
E_1A1Ac	35	19.9	4.33	8.18	15.2	6.5	3.56	0.395	209	350	1.76	1.78
E_2A1Ac	39.7	20.2	6.21	8.15	12	4.1	4.31	0.345	222	410	1.97	1.81

obtained from a CaC_2 injection operation (sample E_A1CaC$_2$Ac), whereas the mineralogy of the slags obtained from normal operation practice in an EAF (samples E_1A1Ac and E_2A1Ac) was very similar to the sample E_A1Ac. A comparison between the samples E_A1Ac and E_A1CaC2Ac revealed that the sample E_A1CaC2Ac did not contained γ-Ca_2SiO_4, nor there was any observable quantity of magnesium chromite, whereas it did contain aluminium spinel, mayenite and more noticeable quantities of periclase (Table 2).

Table 2. *Mineral phases identified by XRD and SEM-EDS analysis*

Sample	XRD analysis	Additional mineral phase analysed by SEM-EDS
E_A1Ac	γ-Ca_2SiO_4, $MgCr_2O_4$, β-Ca_2SiO_4, $Ca_2Al_2SiO_7$, $Ca_7Mg(SiO_4)_4$, $Ca_3Mg(SiO_4)_2$	Fe droplets, $CaTiO_3$, MgO, $MgAl_2O_4$, Mn inclusion
E_A2Ac	γ-Ca_2SiO_4, MgO, β-Ca_2SiO_4, $Ca_7Mg(SiO_4)_4$, $MgCr_2O_4$, $Ca_3Mg(SiO_4)_2$, $Ca_{12}Al_{14}O_{33}$	Fe droplets, $CaTiO_3$, $MgAl_2O_4$, $Ca_2Al_2SiO_7$, Mn inclusion, C_4AF
E_A3Ac	$Ca_7Mg(SiO_4)_4$, $Ca_3Mg(SiO_4)_2$, $Ca_2Al_2SiO_7$, MgO	Fe droplets, $MgCr_2O_4$, $CaTiO_3$, $MgAl_2O_4$, Mn inclusion, (Ca,Mg)S $Ca_{12}Al_{14}O_{33}$
E_Fac	γ-Ca_2SiO_4, β-Ca_2SiO_4, $Ca_3Mg(SiO_4)_2$, MgO, $Ca_{12}Al_{14}O_{33}$	Fe droplets, $MgCr_2O_4$, $CaTiO_3$, $MgAl_2O_4$, C_4AF, (Fe,Mg,Mn)O
E_A1CaC$_2$Ac	β-Ca_2SiO_4, $Ca_7Mg(SiO_4)_4$, $Ca_{12}Al_{14}O_{33}$, MgO, $Ca_3Mg(SiO_4)_2$, $MgAl_2O_4$,	Fe droplets, $CaTiO_3$, (Ca,Mg)S
E_1A1Ac	$MgCr_2O_4$, γ-Ca_2SiO_4, β-Ca_2SiO_4, $Ca_2Al_2SiO_7$, $Ca_7Mg(SiO_4)_4$, $Ca_3Mg(SiO_4)_2$	Fe droplets, $CaTiO_3$, MgO, Mn inclusion
E_2A1Ac	$MgCr_2O_4$, β-Ca_2SiO_4, $Ca_7Mg(SiO_4)_4$, $Ca_3Mg(SiO_4)_2$, $Ca_2Al_2SiO_7$	Fe droplets, $CaTiO_3$, MgO, Mn inclusion, C_3A

3.2.1 Dicalcium silicate

Ca_2SiO_4 was identified in the investigated EAF S slags in two polymorphs: larnite (β-Ca_2SiO_4) and shannonite (γ-Ca_2SiO_4). Five of the seven air-cooled slag samples (samples: E_A1Ac, E_A2Ac, E_FAc, E_1A1Ac and E_2A1Ac) disintegrated to a certain extent into powder particles during air cooling.19.6 % of the sample E_A1Ac disintegrated into powder, whereas in the case of samples E_A2Ac and E_FAc the proportion of powder was lower, 5.9 % and 7.0 %, respectively. This proportion was even smaller in the case of samples E_1A1Ac and E_2A1Ac, 4.6 % and 1.6 %, respectively. It is well established that this kind of disintegration is driven by the presence of Ca_2SiO_4 in the slag. This mineral undergoes several phase transformations upon cooling. The transformation of the monoclinic β-polymorph to an orthorombic γ-polymorph is accompanied by a volume expansion of about 12 % [16]. Sample E_A3Ac did not disintegrate into powder due to the absence of β- and γ-Ca_2SiO_4.

The Ca_2SiO_4 in the air-cooled slag sample occurred in a variety of forms, but most frequently as ovoid grains and euhedral laths (Fig. 1). In the case of samples E_A2Ac and E_FAc an elongated shape, with lengths of up to 10 μm, and surrounded by mayenite, was also observed (Fig. 2, right). Observations made on about 100 quantitative electron microprobe analyses of sample E_A1Ac showed that the chromium content in the Ca_2SiO_4 was 0.43 at.%. In the case of other air-cooled slag samples chromium was also found in the Ca_2SiO_4, whereas Shen et al. [15] also found chromium in the silicate phase.

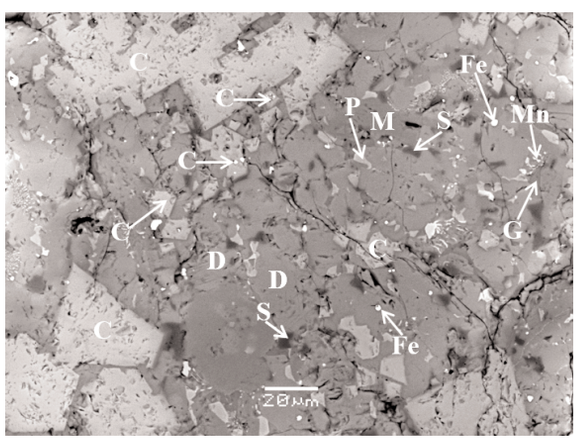

Figure 1. *Microstructures of main mineral phases in the sample E_A1Ac (Key: C-$MgCr_2O_4$, D- Ca_2SiO_4, Fe-Fe droplet, M-$Ca_3Mg(SiO_4)_2$, Mn-Mn inclusion, P-$CaTiO_3$, S-$MgAl_2O_4$)*

3.2.2 Bredigite

Bredigite ($Ca_7Mg(SiO_4)_4$), where partial substitution of calcium by magnesium occurs, was identified in all of the investigated EAF S slag samples, with the exception of sample E_FAc (Table 2). In the case of the air-cooled slag samples bredigite occurred most frequently in the form of ovoid grains. Chromium was also found in the bredigite.

3.2.3 Spinels

The chemical simplified formula for the spinel phase is (Mg^{2+}, Fe^{2+}, Mn^{2+}, Ti^{4+}, Cr^{2+})(Cr^{3+}, Fe^{3+}, Al^{3+})$_2O_4$, and it indicates potential substitutions of different elements in this phase. Spinels crystallise in an octahedral form, and this is why the cross–section of these particles are angular in shape [17]. In samples E_A1Ac, E_1A1Ac, E_2A1Ac and E_A2Ac grey angular spinels predominantly occur as magnesium chromite, being identified by XRD analysis (Table 1).

Otherwise, the group of spinels can be divided into three parts.

The first group of spinels was observed just in the case of samples E_A1Ac, E_1A1Ac, E_2A1Ac and E_A2Ac. Large particles having sizes of about 20 μm tend to form larger magnesium chromite clusters (Fig. 1). The size and clustering of these larger particles indicate that they are present at the process temperature [12; 18-19]. The clusters are formed when individual particles make contact with one another, and become attached to each other in order to lower the total surface energy [18]. Some spinel particles contain numerous metallic particles (Fig. 1). According to Durinck et al. [18], the iron oxide in the spinel decomposes into metallic Fe, thus liberating oxygen, due to the operation process in an EAF at a very low p_{O2}. This reaction occurs predominantly along porous channels in the spinel particles. Partial replacement of Mg^{2+} by Mn^{2+} and Cr^{3+} with Al^{3+} was observed in the particles of magnesium chromite (Fig. 1). Titanium and iron replacement was also found to a smaller extent (less than 0.3 at.%; the results were obtained by approx. 100 analyses in the case of sample E_A1Ac). The replacement was enhanced towards the edge of the grey angular particles. Guo et al. [20] also found that, in the case of EAF slags made from austenitic stainless steel, large quantities of chromium are present as MgO•(Cr, Al)$_2O_3$.

The second group consisted of small magnesium chromite particles, which were only few microns in diameter and were evenly distributed over the slag samples E_A1Ac and E_A2Ac, and unevenly over samples E_A3Ac and E_FAc. Partial replacement of Mg^{2+} by Mn^{2+}, and Cr^{3+} by Al^{3+}, was observed in the case of this group.

The third group consisted of aluminium spinel (Fig. 1-2). The latter appeared in all of the investigated EAF S slags, with the highest content in the sample E_A1CaC$_2$Ac, whereas in others they appeared in smaller quantities, where the minerals were unevenly distributed. Also in the case of the aluminium spinels partial replacement of Al^{3+} by Cr^{3+}, and Mg^{2+} by Mn^{2+}, was observed. Tossavainen et al. [13], also, differentiated a spinel phase from the matrix forming phases in an analysed sample of EAF high alloyed steel slag (3.3 wt.% Cr_2O_3), which was semi-rapidly cooled.

3.2.4 Merwinite

Merwinite $Ca_3Mg(SiO_4)$ crystallized in all the investigated EAF S slags. It typically occurred as an oblong-shaped, laddered structure (Fig. 1). Chromium and manganese were frequently incorporated in the merwinite, occasionally iron, titanium, vanadium, and rarely fluor, sulphur and potassium.

3.2.5 Gehlenite

Gehlenite ($Ca_2Al_2SiO_7$) was found in almost all of the investigated EAF S slags, except in samples E_FAc and E_A1CaC$_2$Ac. The highest quantity was found in sample E_A3Ac. Gehlenite is xenomorphic and fills the space between grains of dicalcium silicate or grains of merwinite and spinel (Fig. 1-2). It rarely crystallizes in a pure form, and often manganese and chromium are detected in gehlenite particles, occasionally iron and titanium. Gehlenite occurs typically in paragenesis with bright manganese

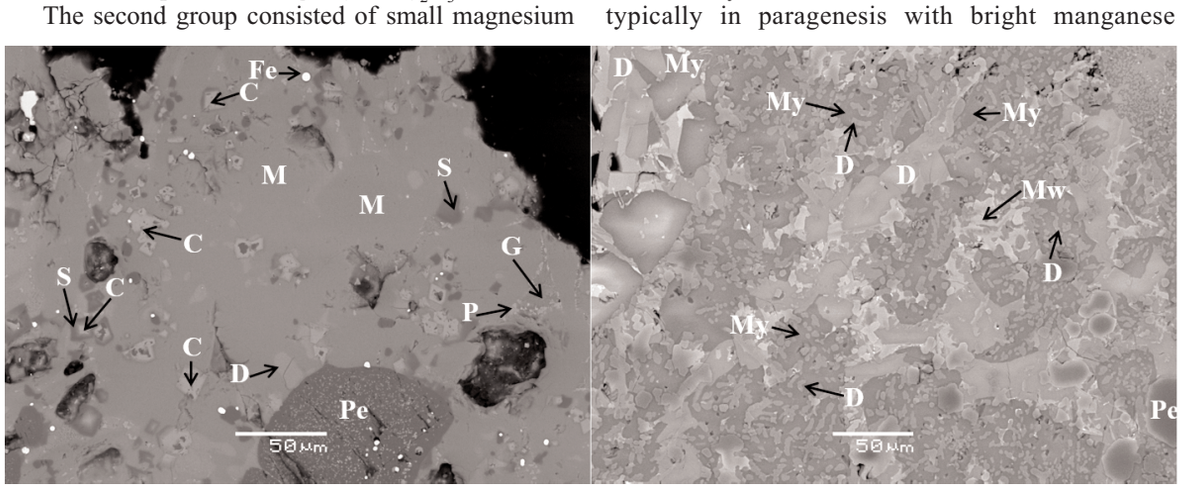

Figure 2. *Microstructures of main mineral phases in the sample E_A3Ac (left) and E_FAc (right) (Key: C-$MgCr_2O_4$, D-C_2S, Fe-Fe droplet, M-$Ca_3Mg(SiO_4)_2$, My-$Ca_{12}Al_{14}O_{33}$, Mw-(Fe,Mg,Mn)O, Pe-MgO, S-$MgAl_2O_4$)*

inclusions (Fig. 1-2), which have a high content of sulphur, and iron and chromium are frequently found in such inclusions. Some grains containing fluoride were also found.

3.2.6 Mayenite

Mayenite ($Ca_{12}Al_{14}O_{33}$) appeared just in samples E_A2Ac, E_FAc and E_A1CaC_2Ac. Like gehlenite, mayenite is xenomorphic, and usually fills the space between Ca_2SiO_4 (Fig. 2, right). It is rarely crystallized in a pure form, and chromium and manganese are often incorporated in the mayenite structure. Bradaškja et al. [21], too, found mayenite in EAF S slags.

3.2.7 Periclase

More noticeable amounts of periclase (MgO) were found in samples E_A2Ac, E_A3Ac, E_FAc and E_A1CaC_2Ac (Table 2). Typically periclase was evenly distributed in the air-cooled EAF S slags. It usually occurred in the form of cubic crystals, with lengths of between 30 μm and 250 μm, and widths of between 20 μm and 100 μm. Some grains of periclase contained metallic particles (Fig. 2).

3.2.8 Other mineral phases

SEM-EDS analyses of the air-cooled slag sample revealed the presence of some other mineral phases, which could not be confirmed by means of XRD analyses, due to the small quantities of these minerals.

3.2.8.1 Perovskite

The small, less than 10 μm large, sickle-shaped, smooth, poreless, unevenly distributed bright particles belong to perovskite ($CaTiO_3$) (Fig. 1), which was found in all of the investigated EAF S slags. Niobium, chromium, manganese, and rarely barium and vanadium, are incorporated into the structure of perovskite. The general chemical formula of perovskite has been reported as (Ca, Mg, Al, Fe)(Ti, Al, Si)O_3 [22]. It has also been reported that the precipitation and growth of perovskite crystals is promoted by increased slag basicity (CaO/SiO_2 > 1.55) [23], which is in agreement with our findings, The slag basicity of the investigated air-cooled EAF S slags, defined as the ratio CaO/SiO_2 in wt%, was, on average, 2.

3.2.8.2 Brownmillerite

Just a few crystals of brownmillerite (Ca_2(Al, Fe)$_2O_5$) (C_4AF) were found, just in samples E_A2Ac and E_FAc. Such crystals typically fill the space between particles of Ca_2SiO_4. Titanium, chromium, manganese, and rarely barium and vanadium, are usually found in brownmillerite.

3.2.8.3 RO phase

A solid solution of (Fe, Mg, Mn)O was found just in sample E_FAc. It was unevenly distributed in the sample, typically as bright round-shaped crystals with dimensions of up to 70 μm, and sometimes as elongated narrow crystals (Fig. 2, right). Tossavainen et al. [13] and Bradaškja et al. [21], too, found such crystals in an EAF slag solid solution.

3.2.8.4 Oldhamite

Just few crystals of oldhamite (Ca, Mg)S were found in samples E_A2Ac and E_A1CaC_2Ac. They had dimensions of just a few μm, and were very bright.

3.2.9 Iron droplets

The microstructure of all of the investigated EAF S slags also revealed spherical metallic droplets, which were unevenly distributed throughout the slag samples. The microstructure of these droplets was investigated in detail in the case of sample E_A1Ac.

In sample E_A1Ac two kinds of spherical metallic droplets could be distinguished. The first group consisted of large spherical droplets with sizes of up to 250 μm. The second group contained mainly smaller particles with a maximum diameter of 5 μm, which were encountered in large amounts in the slag. Droplets with diameters of more than 5 μm have a composition which is comparable to that of the austenitic stainless steel X2 CrNi 19–8, containing mainly iron, chromium and a small amount of nickel. This is in agreement with the findings of Durinck et al. [18], and Durnick et al. [24], who reported that large droplets were found in austenitic stainless steel slag with a composition comparable to that of stainless steel. The large spherical droplets originated from the steel bath. These spherical droplets were most likely splashed from the melt bath into the slag layer during the melting process by falling scrap [12; 18]. It has been reported that, in the metallurgical process, electrode heating has a strong effect on the splashing of droplets into the slag layer [19].

The majority of the small droplets (<5 μm) contained more than 90 wt.% of iron, the rest being chromium. It can be presumed that droplets of the second kind do not originate from the metallic bath, but are formed inside the slag itself [18; 24].

3.3 Physico-mechanical characterisation of EAF S slags

All the investigated slag samples were coarse, with more than 75 % slag particles having sizes of more than 1 mm. Irrespective of the water cooling treatment mode the water-cooled slags had, in general, slight bigger particles in comparison to the air-cooled slags (Table 3).

Table 3. *Particle size distribution of air- and water-cooled slag samples obtained from normal operation practice in an EAF and from CaC_2 injection operation*

	Procent passing (mass %)								
Grain size (mm) Sample	0.063	0.125	0.25	0.5	1	2	4	8	11.2
E_1A1Ac	8	12	14	18	24	34	50	92	100
E_1A1Wi	3	5	7	10	15	25	44	94	100
E_1A1Wq	3	5	7	10	14	24	43	95	100
E_A1CaC$_2$Ac	1	2	4	8	14	27	49	95	100
E_A1CaC$_2$Wi	2	3	4	8	14	25	45	95	100
E_A1CaC$_2$Wq	1	1	3	5	10	20	396	94	100

Cooling treatment: Ac = air cooling; Wi = immersion; Wq = quenching

In the case of samples E_A1CaC2Ac, E_A1CaC$_2$Wi and E_A1CaC$_2$Wq the average compact density was 3.73 Mg m^{-3}, whereas in the case of samples E_1A1Ac, E_1A1Wi and E_1A1Wq it was 4.04 Mg m^{-3}, so it was in both cases a bit higher than in the study by Tossavainen et al. [13], where the compact density for high-alloy steel slag was 3.34 Mg m^{-3}. The results of measurements showed no noticeable differences in compact density between the different size fractions of the material (f.0/4 and f.4/10), the method of water cooling treatment (immersion/quenching), the different cooling treatment (air/water cooling), and the different technological processes used to make slag in an EAF (reduction by CaC_2 vs. FeSi).

It was observed that the BET surface of f. 0-1 was higher than that of f. 1-4. Also, the BET surface was higher, in the case of the water-cooled slags, irrespective of the water cooling treatment, than the values for the air-cooled slag samples and, in general, the BET surface of slags produced at normal operation practice was greater than at CaC_2 injection trial (Table 4). The average pore diameter of the samples produced by means of CaC_2 injection trial was 15.1 nm, whereas in the case of the samples produced by the normal operation practice it was somewhat greater, 18.8 nm, in both cases irrespective of the cooling treatment and the slag fraction (Table 4).

Table 4. *BET surface and average pore diameter of the investigated EAF S slags. The average pore diameter (4V/A) was calculated from the desorption part of the curve*

Sample	*fraction/*	*m/*	*BET/*	*Average pore diameter /*nm*
	mm	g	m^2 g^{-1}	
E_A1CaC2Ac	0–1	8.74	0.098	15.09
	1–4	13.84	0.0172	16.15
E_A1CaC2Wi	0–1	14.39	0.2865	18.09
	1–4	10.49	0.1255	13.38
E_A1CaC2Wq	0–1	2.61	0.131	17.27
	1–4	8.13	0.061	10.46
E_1A1Ac	0–1	9.73	0.3625	18.45
	1–4	11.39	0.0865	23.07
E_1A1Wi	0–1	10.81	0.4187	17.9
	1–4	8.59	0.1264	18.97
E_1A1Wq	0–1	8.29	0.4534	18.41
	1–4	9.64	0.1297	15.92

3.4 The mineral phases in the water-cooled EAF S slags

The same main mineralogical phases were identified in the air-cooled slag sample as in the water-cooled slag samples, by means of XRD and SEM-EDS analysis. Based on Mostafaee et al. [12] calculation, who had reported that the first crystalline phase which precipitate from liquid slag is magnesiochromite, followed by dicalcium silicate and calcium magnesium silicate at around 1735 K (1460 °C), was concluded that in the water-cooled slags the main mineral phases (chromite, merwinite, dicalcium silicate…) were probably already formed before water cooling treatment.

Comparison of XRD analysis of air- and water-cooled slag samples before and after exposure to the down-flow column test reveal same main mineralogical phases, which indicate that during the column test chemical reaction (dissolution of minerals, precipitation of secondary minerals…) primarily took place on the slag surface.

The crystalline nature of the air- and water-cooled EAF S slag samples was probably due to the high basicity index (Mb) of the investigated EAF S slags (which was, on average, 1.8). Tossavainen et al. [13], too, found that EAF slags consist largely of crystalline

materials, despite rapid water cooling, and slags with Mb > 1 result in mainly crystalline slags.

However, the water cooling treatment of slags lead to absence of γ-Ca_2SiO_4 and precipitation of secondary mineral phases.

The absence of γ-Ca_2SiO_4 in the water-cooled slag sample was confirmed by the XRD path as being most likely due to the cooling conditions (rapid water cooling treatment) [25] or dissolution of γ-C_2S in the cooling water [26]. Also in the air-cooled slag after the exposure to the down-flow column test (sample E_A1Ac*) the absence of γ-Ca_2SiO_4 was confirmed by the XRD path. Engström et al. [26] found good solubility of γ-Ca_2SiO_4 at alkaline pH. In the XRD of accelerated carbonated steel slag decrease of intensity of γ-Ca_2SiO_4 was reported by Diener et al. [27], which indicates on good solubility of γ-Ca_2SiO_4. In the water-cooled slags no disintegration into powder was observed, which indicates their volumetric stability.

The conditions during water cooling treatment (exposure to water, the slags with high surface temperatures were in contact with the water) accelerated the precipitation of secondary mineral phases onto the surfaces of the slag particles. It was also observed that the variation in the method of water cooling treatment did not lead to different formations of secondary mineral phases.

Precipitation of the secondary formed mineral phases was also observed in the slag samples after exposure to the down-flow column test. From the mineralogical point of view, the same secondary mineral phases were formed during the down-flow column test in the water-cooled sample E_A1Wq* as in the case of the air-cooled sample E_A1Ac*.

Portlandite and calcite were the most common secondary mineral phases in the water-cooled slags. XRD diffractograms of samples E_FAc, E_2A1Wi1, E_2A1Wi2, E_2A1Wq revealed the presence of portlandite, whereas in samples E_A2Wi and E_A3Wq, E_A1CaC_2Wi and E_A1CaC_2Wq precipitation of calcite was observed (Table 5). In the case of SEM-EDS analysis it was not possible to distinguish between portlandite and calcite. However, due to the fact that portlandite and calcite were also found by XRD analysis, the assumption was made that portlandite was also identified by SEM-EDS analysis in samples E_FAc, E_2A1Wi1, E_2A1Wi2, E_2A1Wq1 and calcite in the samples E_A1Ac, E_A2Wi and E_A3Wq, E_A1CaC_2Wi and E_A1CaC_2Wq.

Since the investigated EAF S slags did not contain free lime, the portlandite and calcite precipitation probably occurred through the dissolution of calcium silicates. Van Zomeren et al. [28] reported that CSH (calcium silicate hydrate) and portlandite are formed after dissolution of Ca_2SiO_4. The carbonation reaction probably take place in two subsequent step: calcium was first leached from the Ca-minerals and subsequently reacted with dissolved carbonate to form calcite. This mechanism of carbonation have also been observed by van Zomeren et al. [28] and Huijgen et al. [29]. In the water-cooled slag samples and in the slag samples exposed to the down-flow column test microcracks due to dissolution processes were observed, predominantly on the surface of individual Ca_2SiO_4 grains, or slightly beneath the surface of these grains (Fig. 3, left) and the formation of rosette shaped calcite on the slag surface (Fig. 3, right). However, during water cooling treatment and during the down-flow column test carbonation occurred to a much smaller extent than during the accelerated carbonation of the slag [28-30], due to the larger slag particles of the investigated samples, and a lower CO_2 uptake from the atmosphere.

Table 5. *Secondary mineral phases in the water-cooled samples and in the samples exposed to the down-flow column test*

Sample	XRD analysis	SEM-EDS analysis
E_A1Wq	/	$CaCO_3$, ettringite
E_A2Wi	$CaCO_3$	ettringite, CAH
E_A3Wq	$CaCO_3$	ettringite
E_FWq	$Ca(OH)_2$, SiO_2, $CaSO_4 \cdot 2H_2O$	ettringite, CAH
E_A1CaC_2Wi	$CaCO_3$	ettringite, CSH, CAH
E_A1CaC_2Wq	$CaCO_3$	CSH
E_1A1Wi	/	CAH
E_1A1Wq	/	ettringite, CAH
E_2A1Wi1	$Ca(OH)_2$	ettringite, CAH
E_2A1Wi2	$Ca(OH)_2$	CSH, CAH, $Ca(OH)_2$
E_2A1Wq1	$Ca(OH)_2$	$Ca(OH)_2$
E_2A1Wq2	/	/
E_A1Ac*	*$CaCO_3$	ettringite
E_A1Wq*	*$CaCO_3$	ettringite

**XRD analysis of the crystals on the surface of the slag particles*

SEM-EDS observations of polished slag grains indicated the formation of another secondary, sulphur-rich mineral belonging to the calcium sulfoaluminate hydrate group. On the surface of the water-cooled slag particles secondary sulphur-rich minerals occurred with a needle-like morphology, just a few μm wide, and about 40 μm long, whereas more frequently secondary sulphur-rich minerals were observed in the voids in the form of short, clumped, prismatic crystals (Fig. 4). Mapping of these crystals, performed on polished slag grains, indicated that sulphur was

concentrated in the middle of the needle formation, whereas the surrounding area was enriched by calcium and silicon (Fig. 5)

The observed minerals in the air-cooled slag after exposure to column test (sample E_A1Ac*) most frequently have a needle-like structure, with lengths of between 20 μm and 50 μm, and widths of approximately 5 μm, whereas in water-cooled slag after exposure to column test (sample E_A1Wq*) more frequently in the voids in the form of short, clumped crystals, but rarely in the form of needles on the surface of particles. It was also observed that some larger metallic droplets had fallen out of the slag sample after the test, and that the empty holes were filled up with observed minerals. The incorporation of chromium in the needle or clumped structure was frequently observed in the newly-formed minerals. Taking into account the morphology of all these crystals and the chemical analysis results obtained by EDS, all these minerals are, in all probability, ettringite ($Ca_6[Al(OH)_6]_2(SO_4)_3 \cdot 26H_2O$). Ettringite is a hydrous calcium alumina-sulfate mineral, which is

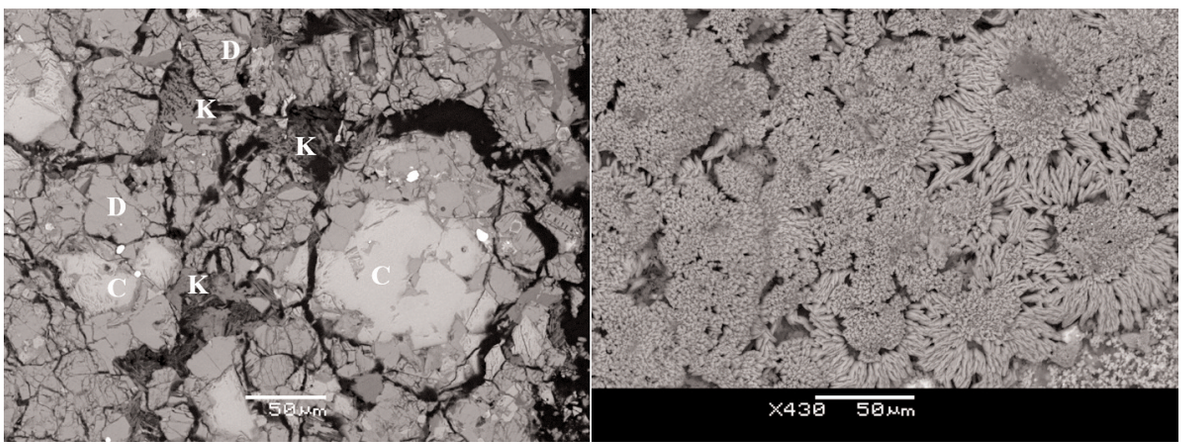

Figure 3. *The observed microcracks and the precipitation of calcite on the polished sample E_A1Wq* (left) (Key: D-C_2S, C-$MgCr_2O_3$, K-$CaCO_3$) and the the formation of rosette-shaped calcite on the unpolished surface of the sample E_A1Wq* (right)*

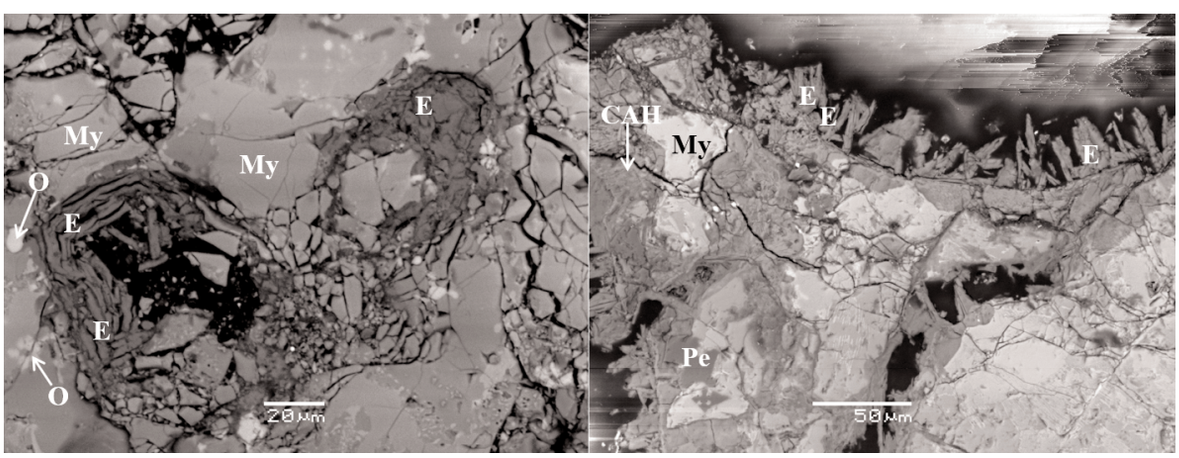

Figure 4. *Precipitation of ettringite in sample E_A2Wi (left) and precipitation of CAH and ettringite in sample E_FWq (right) (Key: CAH-calcium aluminate hydrate, E-ettringite, My-$Ca_{12}Al_{14}O_{33}$, O-(Ca,Mg)S)*

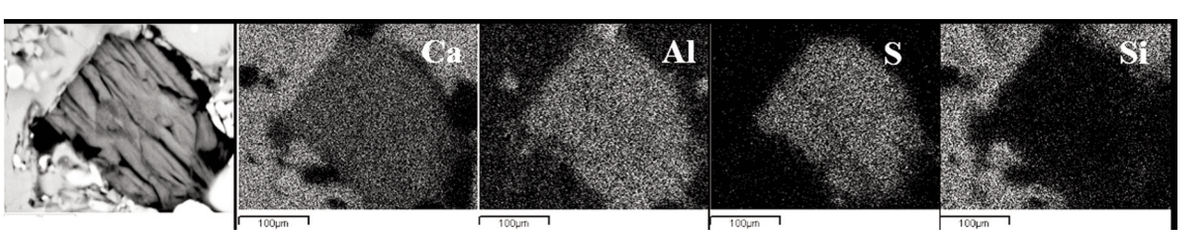

Figure 5.*Mapping of ettringite in the sample E_A1Wq*

precipitated in environments with a high pH and a high sulfate activity [31]. Several authors have pointed out the possibility of SO_4^{2-} substitution by oxyanions, such as CrO_4^{2-} and MoO_4^{2-} [32-35]. It has been frequently postulated that solid solution formation in ettringite is a controlling mechanism for oxyanion leaching [36], for example in the case of Cr(VI) in cement [37].

Dissolution of mayenite and the precipitation of calcium aluminate hydrate (CAH) was observed in samples E_A2Wi, E_FWq and E_A1CaC$_2$Wi (Table 5, Fig. 4, right), where XRD analysis revealed the presence of mayenite. To a much smaller extent precipitation of CAH was also observed in the water-cooled slag samples E_1A1Wi, E_1A1Wq, E_2A1Wi1 and E_2A1Wi2. Mayenite is highly hydraulic, and reacts very quickly with water [26; 38–39]. The results of such hydration is unstable hydrate C_2AH_8, which will later changes into the thermodynamic stable form of C_3AH_6 [38; 40]. The presence of CAH has not been confirmed by XRD analysis, since the CAH is poorly crystalline.

CSH (calcium silicate hydrate) was frequently observed in the water-cooled slag samples. The precipitation of CSH occurred through the dissolution of calcium silicates, which have been also reported by van Zomeren et al. [28] and Kriskova et al. [41]. The presence of CSH has not been confirmed by XRD analysis, since the CSH is poorly crystalline [42].

The sulphur content in sample E_FWq (w = 0.417±0.003 %) was higher than in the other investigated EAF S slags (from 0.095 wt.% to 0.296 wt.%), which was probably the reason for the precipitation of gypsum. It has to be noted that just a small amount of gypsum is revealed in the diffractogram corresponding to sample E_FWq.

Upon water cooling treatment no hydration of periclase occurred, although later on, upon exposure to the atmosphere, hydration and carbonation of periclase can also occur.

4. Conclusions

The XRD patterns of the investigated EAF S slags are very complex, with several overlapping peaks resulting from the many minerals present in investigated samples. A certain variation of the mineralogy of the EAF S slags coming from different steel grades was observed. It was also shown that the technological processes of steel production in an EAF have a significant effect on slag mineralogy.

The mineral phases identified by XRD and SEM in the investigated EAF S slags were determined to be:

- sharp-cornered magnesium chromite, with the partial replacement of Mg^{2+} by Mn^{2+} , and Cr^{3+} by Al^{3+} (enhanced at the edge of the particles), and sharp-cornered aluminium spinel,
- ovoid grains and euhedral laths of dicalcium silicate, appearing as larnite or shannonite,
- ovoid grains of bredigite,
- oblong, ladder-shaped grains of merwinite,
- xenomorphic gehlenite and mayenite,
- cubic crystals of periclase (MgO),
- large spherical metallic droplets with sizes of up to 250 μm and small metallic droplets with a maximum diameter of 5 μm,
- small quantities of perovskite ($CaTiO_3$), brownmillerite, oldhamite (Ca, Mg)O and RO phase (Fe, Mg, Mn)O.

Chromium was frequently incorporated in all the main mineral phases.

The results of the study have shown that water cooling treatment quenching did not prevent the crystallization of mineral phases, probably due to the high basicity of the investigated EAF S slags. Nevertheless, water cooling treatment has an effect on the formation of secondary minerals, calcite, portlandite, ettringite, calcium aluminate hydrate and calcium silicate hydrate. In the air- and water-cooled slags after exposure to the down-flow column test the same secondary mineral phases (calcite, ettringite) were formed as during the water cooling treatment. From the point of view of leaching, these minerals are very important, since they control the leaching process of the trace elements.

From the mineralogical point of view, the investigated water-cooled EAF S slags have the potential for use in road bases in the bound form, or in combination with other hydraulic binders. Nevertheless, before EAF S slags can be used, they should be evaluated on a case-by-case basis, since their mineralogy varies considerably. On the other hand, their environmental and technical aspects need to be fully investigated.

Acknowledgement

The operational part of this study was financed by the European Union, European Social Fund. Operation was implemented within the framework of the Operational Programme for Human Resources Development for the Period 2007–2013, Priority axis 1: Promoting entrepreneurship and adaptability, Main type of activity 1.1.: Experts and researchers for competitive enterprises.

References

[1] Euroslag 2012, Position paper on the status of ferrous slag complying with the waste framework directive (article 5/6) and the REACH regulation, Duisburg-Rheinhausen, 2012.

[2] D. Durinck, F. Engström, S. Arnout, J. Heulens, P.T. Jones, B. Björkman, B. Blanpain, P. Wollants, Resour. Conserv. Recy., 52 (2008) 1121–1131.

[3] H. Motz, J. Geiseler, Waste. Manage. 21 (2001) 285–293.

[4] D.S. Apul, K.H. Gardner, T. Taylor Eighmy, A.-M. Fällman, R.N.J. Comans, Environ. Sci. Technol., 39 (2005) 5736–5741.

[5] European Commission, Research fund for Coal and Steel, Energy and productivity optimised EAF stainless steel making by adjusted slag foaming and chemical energy supply (EPOSS), G. Stubbe, G. Harp, A. Jaklič, M. Sedlmeier, T. Rodriguez Duran, final report, Luxembourg, 2013.

[6] SIST EN 12457-4:2004, Characterisation of waste - Leaching - Compliance test for leaching of granular waste materials and sludges - Part 4: One stage batch test at a liquid to solid ratio of 10 l/kg for materials with particle size below 10 mm (without or with size reduction)

[7] M. Loncnar, M. Zupančič, P. Bukovec, A. Jaklič, Mater. Tech., 43 (2009) 315– 321.

[8] USEPA (2008) Method 1312, Synthetic precipitation leaching procedure.

[9] SIST EN 933-1:1999/A1:2005, Tests for geometrical properties of aggregates - Part 1: Determination of particle size distribution - Sieving method.

[10] SIST EN 1097-7:2008, Tests for mechanical and physical properties of aggregates - Part 7: Determination of the particle density of filler - Pyknometer method.

[11] ISO 15901-2:2006, Pore size distribution and porosity of solid materials by mercury porosimetry and gas adsorption -- Part 2: Analysis of mesopores and macropores by gas adsorption.

[12] S. Mostafaee, M. Andersson, P. Jönsson, 27 (2010) 425–436.

[13] M. Tossavainen, F. Engstrom, Q. Yang, N. Menad, M. Lidstrom Larsson, B. Bjorkman,Waste. Manage. 27 (2007) 1335–1344.

[14] B. Vidacak, I. Arvanitidis, P.G. Jönsson, P. Sjöberg P., Scand. Journal. Metall., 31 (2002) 321–327.

[15] H. Shen H, E. Forssberg E, U. Nordström, Resour. Conserv. Recycl., 40 (2004) 245–271.

[16] Y.J. Kim, S.K. Kim, D.S. Kim, Y.D. Lee, P.K. Yang, J. Am. Ceram. Soc., 75 (1992) 2407–2419.

[17] R. Dekkers, C.F. Woendregt, P. Wollants, J. Non-Cryst. Solids., 282 (2001) 49–60.

[18] D. Durinck, P.T. Jones, M. Guo, F. Verhaeghe, G. Heylen, R. Hendrickx, R. Baeten, B. Blanpain, P. Wollants, Steel Res. Int., 78 (2007) 125–135.

[19] J. Ekengård, A.M.T. Andersson, P.G. Jönsson, Ironmaking Steelmaking, 35 (2008) 575–588.

[20] M. Guo, D. Durinck, P.T. Jones, G. Heylen, R. Hendrickx, R. Baeten, B. Blanpain, P. Wollants, Steel Res. Int., 78 (2007) 117–124.

[21] B. Bradaškja, J. Triplat, M. Dobnikar, B. Mirtič, Mater. Tech. 2004; 38 (2004) 205–208 (in Slovenian language).

[22] L. Zhang, L. Zhang, M. Wang, G. Ki, Z. Sui, ISIJ Int., 46 (2006) 458–465.

[23] J.W. Kim, S.K. Kim, D.S. Kim, X.D. Lee, P.K. Yang, ISIJ Int., 36 (1996) 40–43.

[24] D. Durnick, P.T. Jones, B. Blanpain, P. Wollants, J. Amer. Ceram. Soc., 91 (2008) 3342–3348.

[25] C.J. Chan, W.M. Kriven, J.F. Young, J. Am. Ceram. Soc., 75 (1992) 1621–1627.

[26] E. Engström, D. Adolfsson, Q. Yang, C. Samuelsson, B. Björkman, Steel Res. Int., 81 (2010) 362–371.

[27] S. Diener, L. Andreas, I. Herrmann, H. Ecke, A. Lagerkvist, Waste Manage., 30 (2010) 132–139.

[28] A. Van Zomeren, S.R. van der Laan, H.B.A. Kobsen, W.J.J. Huijgen, Waste Manage., 21 (2011) 2236–2244.

[29] W.J.J. Huijgen, H.-J. Witkamp, R.N.J. Comans, Environ. Sci. Technol., 39 (2005) 9676–9682.

[30] P. Suer P, J.E. Lindqvist JE, M. Arm M, P. Frogner–Kockum, Sci. Tot. Environ., 407 (2009) 5110–5118.

[31] R.B. Perkins, C.D. Palmer, Geochim. Cosmochim. Acta, 63 (1999) 1203–1218.

[32] M. Zhang M, E.J. Reardon, Environ. Sci. Technol., 37 (2003) 2947–2952.

[33] M. Chrysochoou, D. Dermatas, J. Hazar. Mater., 136 (2006) 20–33.

[34] H. Pöllman, S. Auer, H.J. Kuzel, Cem. Concr. Res., 23 (1993) 422–430.

[35] R.B. Perkins, C.D. Palmer, Appl Geochem., 15 (2000) 1203–1218.

[36] G. Cornelis, C. Anette Johnson, T. Van Gerven, C. Vandecasteele, Appl. Geochem., 23 (2008) 955–976.

[37] M. Ochs M, B. Lothenbach B, E. Giffaut, Radioch. Acta, 90 (2002) 639–646.

[38] D. Adolfsson, R. Robinson, F. Engström, B. Björkman, Cem. Concr. Res., 41 (2011) 865–871.

[39] D. Adolfsson, F. Engström, R. Robinson, B. Björkman, Steel Res. Int. 2011; 82 398–403.

[40] Y. Fu, J. Ding, J.J. Beaudoin, Cem. Concr. Res., 26 (1996) 417–426.

[41] L. Kriskova ,Y. Pontikes, Ö. Cizer, G. Mertens, W. Veulemans, D. Gesen, P.T. Jones, L. Vanderwalle, K. van Balen, B. Blanpain, Cem. Concr. Res., 42 (2012) 778–788.

[42] L. Muhmood L, S. Vitta S, D. Venkateswaran, Cem. Concr. Res. 2009; 39 (2009) 102–109.